Research Square

Preprints are preliminary reports that have not undergone peer review.
They should not be considered conclusive, used to inform clinical practice,
or referenced by the media as validated information.

Strong and Programmable Dry Adhesion through Graded Modulus Design

K. Jimmy Hsia

kjhsia@ntu.edu.sg

Nanyang Technological University https://orcid.org/0000-0003-3065-3769

Yangchengyi Liu

Nanyang Technological University https://orcid.org/0009-0003-8291-4980

Yuning Yang

Nanyang Technological University

Yingjie Fu

Nanyang Technological University

Weiyi Liu

Xiangtan University

Shengzhe Hong

Nanyang Technological University

Boaz Sing Hao Teo

Nanyang Technological University

Xudong Yang

Nanyang Technological University

Wentao Ke

Nanyang Technological University

Yingying Zhang

Nanyang Technological University

Estella Yuze Guo

University of Melbourne

Hongjun Yu

Harbin Institute of Technology

Xiufeng Wang

Xiangtan University

Eduard Arzt

INM - Leibniz Institute for New Materials https://orcid.org/0000-0002-0834-4540

Changhong Linghu

City University of Hong Kong

Article

Keywords:

Posted Date: February 12th, 2026

DOI: https://doi.org/10.21203/rs.3.rs-8723773/v1

License: This work is licensed under a Creative Commons Attribution 4.0 International License.
Read Full License

Additional Declarations: There is **NO** Competing Interest.

Strong and Programmable Dry Adhesion through Graded Modulus Design

Yangchengyi Liu[a,b,#], Yuning Yang[a,c,#], Yingjie Fu[a#], Weiyi Liu[a,b], Shengzhe Hong[a], Boaz Sing Hao Teo[a], Xudong Yang[d], Wentao Ke[a], YingYing Zhang[a], Estella Yuze Guo[e], Hongjun Yu[c], Xiufeng Wang[b], Eduard Arzt[a,f,g], Changhong Linghu[h,*], K. Jimmy Hsia[a,i,*]

[a] School of Mechanical and Aerospace Engineering, Nanyang Technological University, 50 Nanyang Avenue, Singapore 639798, Singapore

[b] Key Laboratory of Low Dimensional Materials and Application Technology of Ministry of Education, School of Materials Science and Engineering, Xiangtan University, Xiangtan 411105, China

[c] Department of Astronautic Science and Mechanics, Harbin Institute of Technology, Harbin, 150001, China

[d] Singapore Institute of Manufacturing Technology (SIMTech) Agency for Science, Technology and Research (A*STAR), 2 Fusionopolis Way, Singapore, 138634 Singapore

[e] Department of Mechanical Engineering, the University of Melbourne, Victoria 3010, Australia

[f] INM–Leibniz Institute for New Materials, Campus D2 2, 66123 Saarbrücken, Germany.

[g] Program in Materials Science and Engineering, Jacobs School of Engineering, University of California San Diego, 9500 Gilman Drive, La Jolla, CA 92093, USA

[h] Department of Mechanical Engineering, College of Engineering, City University of Hong Kong, 999077, Hong Kong, China.

[i] School of Chemistry, Chemical Engineering and Biotechnology, Nanyang Technological University, 50 Nanyang Avenue, Singapore 639798, Singapore.

# These authors contributed equally

*Corresponding author: clinghu@cityu.edu.hk (C. L.); kjhsia@ntu.edu.sg (K. J. H.)

Abstract: Strength of soft adhesives is limited by interfacial stress concentrations at corners and edges, which hinder the full utilization of their load-bearing capability. Here, we propose a new class of scalable, compliant graded modulus adhesives (GMAs) that improve strengths by one-order-of-magnitude, extend size limitation of soft adhesives by three-orders-of-magnitude, enable adaption to various surface morphologies, and provide on-demand detachment. We fabricate the GMAs by differential photopolymerization via light attenuation, generating continuous modulus gradient of two-orders-of-magnitude over a 1 mm thick sample, and resulting in glassy and rubbery phase on opposing surfaces. The GMAs effectively homogenize the interfacial stresses over the entire contact surface, eliminate stress concentrations at corners and edges, and enable adhesion at theoretical limit. Upon heating to 80 ℃, the modulus gradient is diminished, leading to drastically lower adhesion strength and easy detachment. These advantages establish GMAs as new adhesive design paradigm for developing next-generation soft adhesives.

Introduction

Robust and strong adhesion is essential for a wide range of engineering applications [1-4]. Adhesion strength is dictated by interfacial fracture, in which suppression of crack propagation is critical [5-8]. Animals such as geckos, spiders, and beetles have evolved fibrillar attachment systems, with structural features from a few hundred nanometers to a few micrometers, to achieve strong, reliable and switchable adhesion [9-11]. Adhesion mechanisms in animals are described by the JKR-DMT transition, where the Johnson-Kendall-Roberts (JKR) model describes edge-stress-dominated detachment and the Derjaguin-Muller-Toporov (DMT) model corresponds to uniform detachment. Submicron- to micrometer-scale fibrils operate in a DMT-like regime and approach near-theoretical adhesion strength through uniform detachment [12-15], whereas larger fibrils detach in a JKR-like regime in which edge stress concentration drives crack propagation and weakens adhesion [16-17]. This intrinsic size dependence fundamentally limits the scalability of fibrillar adhesion, hindering the translation of DMT-like strong adhesion from intricate biological microstructures to practical macroscopic adhesive devices.

To achieve high load-bearing capability, biomimetic micropillar-array adhesives have been developed based on the contact-splitting principle to enhance adhesion strength [18-19]. However, the effective adhesion strength of these arrays does not scale linearly with pillar number because of interfibrillar mechanical interactions and deformation of the backing layer [20-22]. Moreover, such arrays are expensive to fabricate over large areas and are vulnerable to pillar lateral collapse, bundling, and abrasion [23-25]. Therefore, there is a critical need for adhesive systems that preserve DMT-like strong adhesion at meso- or macroscale.

Several structural designs have been proposed to overcome the size limitation of fibrillar, including mushroom-shaped pillars [26-30], soft tip layers[31-33], stiff-base [31-33] or stiff-core [34-36] composites, and continuous stiffness gradients along axial [37] and radial [38] directions. The underlying rationale of these designs is to suppress stress concentrations at the perimeter of the adhesive interface. While these strategies result in much improved adhesive performance, they fall short of achieving uniform stress

distributions at the interface. Materials with large modulus changes (from MPa to GPa range) under external stimulation provide an alternative pathway: in the soft state, they can achieve intimate surface conformity, whereas in the stiff state they suppress local deformation and promote more uniform stress distribution across the interface [13, 24, 39-41]. Based on this principle, the rubber-to-glass (R2G) transition in shape memory polymers (SMPs) enables DMT-like adhesion for a circular contact areas of about 2.5 mm in radius [24]. However, this mechanism requires the full R2G transition to establish strong adhesion, a process that takes several minutes due to slow heat dissipation. Moreover, when switched to the glassy state, the R2G adhesives cannot dissipate energy through viscoelastic deformation, causing interfacial stresses to rise rapidly and making them prone to brittle interfacial failure under minor impacts or vibrations [42]. These limitations significantly restrict the practical applicability of the R2G adhesives and highlight the need for more effective strategies to realize large-scale DMT-like adhesion in soft adhesives.

Materials with graded modulus designs can fundamentally improve interfacial contact and suppress crack initiation [43-44], as exemplified by biological systems such as tooths and tendons. Theoretical models reveal that sufficiently steep modulus gradients reduce the crack-tip driving force, eliminating unstable edge-crack propagation and enabling adhesion that is both flaw-tolerant and size-independent [45-46]. Gradient modulus designs also increase the apparent critical energy release rate [47-48], providing an additional mechanism for improved interfacial toughness. However, these designs have predominantly remained at the theoretical level, with only limited experimental demonstrations to date reporting modulus change of less than one order of magnitude [23, 37], which is insufficient to fully homogenize interfacial stresses and realize scale-independent DMT-like adhesion.

Here we introduce a graded modulus adhesives (GMA) design that incorporates a nearly two orders of magnitude modulus gradient, enabling unprecedented strong and specimen-shape-insensitive adhesion with enhanced surface adaptability. Moreover, the adhesion of the GMA is reversibly switched by a thermally induced phase transition that weakens the modulus gradient. The GMA exhibits excellent flexibility (E_{GMA} =

9.62 MPa; Fig. S1), which allows integration onto transparent flexible substrates such as PET, acrylic, and single-sided tape, and enables scalable fabrication into rolls (Fig. 1A). A continuous through-thickness modulus gradient renders the adhesive soft near the interface to promote conformal contact, but stiff on the backing side to homogenize interfacial stresses, enabling robust adhesion. This design allows the GMA to fully exploit the theoretical adhesion potential across size-scales (Fig. 1B). The normalized adhesion force (F/σ_{th}) of conventional fibrillar adhesives exhibits a pronounced size effect, progressively deviating from the theoretical limit as the apparent contact area increases, even when stress redistribution (e.g. R2G mechanism) or contact splitting strategies are employed. By comparison, GMA consistently operates close to the theoretical adhesion (σ_{th}) limit over contact areas exceeding 1200 mm^2 without splitting the sample into fibrils, extending the scalable regime of strong adhesion by more than 60-fold relative to R2G adhesives and more than 10^8-fold relative to conventional soft fibrils. Beyond suppressing size-effect-induced adhesion loss, the newly developed GMA also allows switching of the interfacial detachment mode (Fig. 1C). Upon heating to 80 °C, a thermally induced phase transition weakens the modulus gradient (Fig. S2), reverting detachment behavior to an edge-initiated mode with reduced adhesion strength.

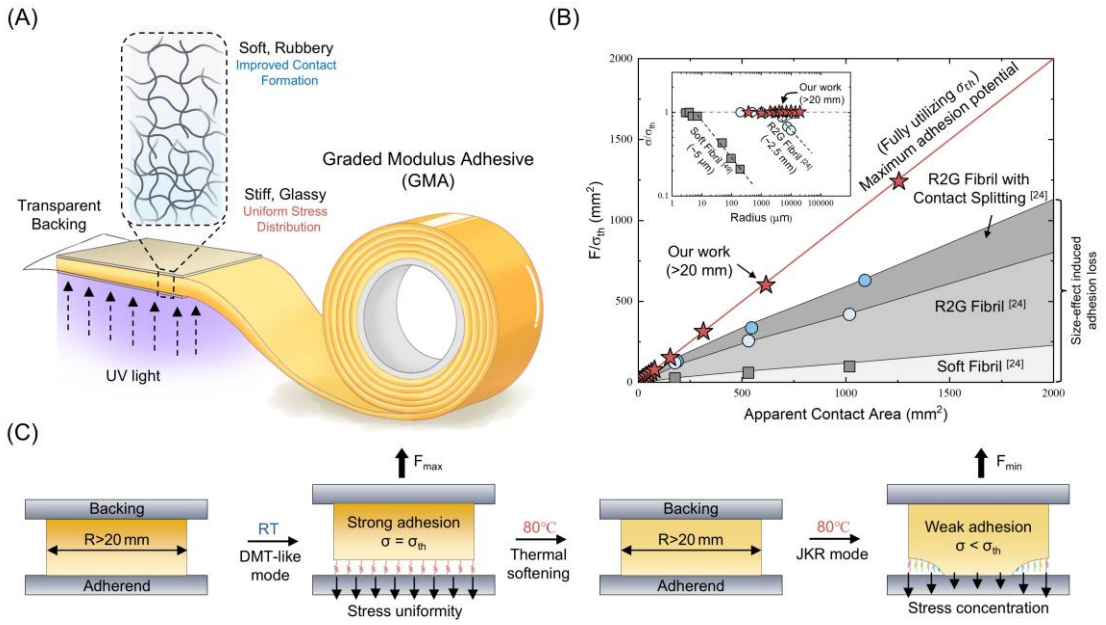


Figure 1. Overview of the graded modulus adhesive (GMA). (A) Schematic of the fabrication of compliant GMAs and their integration with a transparent flexible backing, enabling a rollable adhesive material. (B) Schematic illustration of theoretical adhesion strength (σ_{th}) utilization across increasing contact areas for different adhesive designs. Data for soft fibrils, R2G fibrils, and R2G fibrils with contact splitting are compiled from Ref [24]. The inset compares the JKR-DMT transition as a function of contact radius for different adhesive designs, with data for soft fibrils taken from Ref [49] and data for R2G fibril from Ref [24]. Red star symbols represent data obtained in this work. (C) Schematic illustration of the uniform stress distribution and thermally switchable adhesion enabled by the graded modulus design in GMA.

Materials synthesis and characterization of GMA

The GMA is fabricated by a simple and scalable frontal photopolymerization (FPP) method [50-51], which exploits attenuation of UV light in the photocurable resin to generate a crosslinking density gradient through the thickness direction (Fig. 2A). A photocurable acrylic-based resin is selected because it provides a wide modulus range under varying light intensity. Regions closer to the light source attain higher crosslink density and greater stiffness, whereas those away from the light source show reduced crosslinking and lower stiffness. The concentration of a UV absorber is tuned to control light attenuation within the resin (Fig. S3, Supplementary Note 1), and the samples thickness (z) is precisely controlled by the spacing between the confining substrates. To characterize the crosslink density variation through the thickness, monomer-to-polymer conversion is measured by Fourier transform infrared (FTIR) spectroscopy (Fig. S4, Supplementary Note 2). Under constant light intensity, thicker samples exhibit a larger

difference in the absorption peak of the vinyl C=C bond at 810 cm^{-1} between the top and bottom surfaces, whereas the aromatic sp^2 C-H peak at 840 cm^{-1} remains constant (Fig. 2B). The conversion rate is normalized by the maximum conversion of a fully cured resin, which represents the extent of polymerization and enables comparison across samples of different thickness under same light intensity (Supplementary Note 2). The degree of polymerization at different depths is approximately measured by analyzing samples of different thicknesses and evaluating the conversion ratio at the bottom surface (Fig. 2C). As the sample thickness increases, the normalized conversion decreases because of light attenuation, reaching 0.69 at the bottom surface of a 1-mm-thick sample. Predictions from the FPP model [51] fit the experimental values well (dashed line), validating the method of controlled light attenuation in fabrication of continuously graded crosslink networks.

To quantitatively evaluate the modulus gradient, a series of 150-μm-thick resin thin layers were fabricated to model different depths within a 1-mm-thick GMA. Each layer was polymerized under a specific light intensity estimated by the FPP model to reproduce the local mechanical properties (Fig. S5, Supplementary Note 3). Uniaxial tensile tests were then performed to obtain stress-strain curves (Fig. 2D, E). Young's modulus was calculated from the initial linear stage (strain ≤ 0.3%). At larger depth, modulus decreased significantly as a result of reduced crosslink density. A similar depth-dependent trend was observed when the sample was heated to 80 °C, though the stress level was substantially lower than that at room temperature because the testing temperature exceeded the glass transition temperature (T_g) of the resin (Fig. S6). Figure 2F quantitatively shows the depth-dependent Young's modulus at room temperature (square dot) and 80 °C (round dot). At room temperature, the resin remained in a glassy state, and the modulus decreases exponentially with depth, described by: $E = 235.22 \cdot e^{-3.72 \cdot z} - 4.253$ MPa. At 80 °C, the resin transitions to a rubbery state with enhanced chain mobility, yielding a much slower decay: $E = 299.08 \cdot e^{-0.0057 \cdot z} - 296.27$ MPa. These results demonstrate that FPP can provide a robust and predictable way to fabricate steep and tunable modulus gradients in this material.

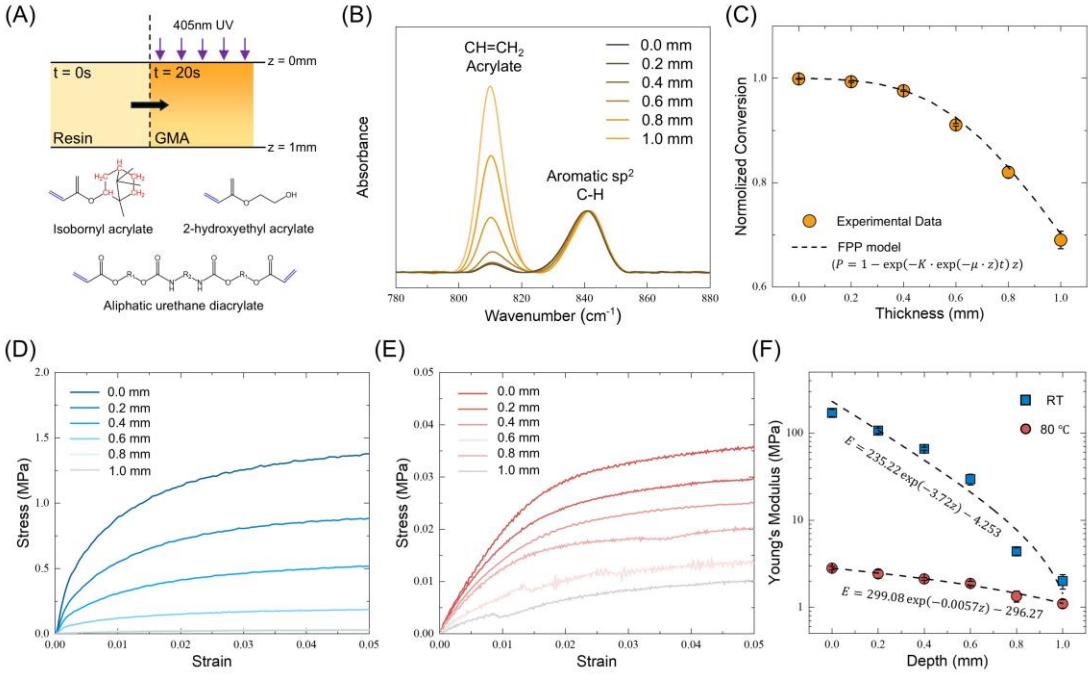


Figure 2. Fabrication and characterization of GMAs. (A) Schematic illustration of the front photopolymerization (FPP) method setup for fabricating thickness-defined GMAs, together with the monomer composition of resin. (B) FTIR spectra of resin films with varying thicknesses. (C) Normalized conversion at the bottom surface as a function of sample thickness, fitted by the FPP model. (D, E) Stress–strain curves of 150 μm resin films fabricated under light intensities corresponding to different depths in a 1 mm GMA sample, measured at room temperature (D) and at 80 °C (E). (F) Young's modulus distribution of GMA in the thickness direction at room temperature (blue) and 80 °C (red).

Weak sample geometry-dependence of GMA adhesion

We investigated the adhesion performance of 1-mm-thick GMA samples with various laser-cut shapes on smooth glass substrates (RMS = 0.0492 μm), using circular samples of different radii (r) as control (Fig. S7, Supplementary Note 4), and compared their performance with other soft adhesives. Pull-off tests conducted on circular GMA, PDMS, and Ecoflex samples with different aspect ratio (r/h) revealed very different detachment behaviors (Fig. 3A, Fig S8). Homogenous soft elastomers, including PDMS and Ecoflex, show a pronounced reduction in adhesion strength with increasing radius because of JKR-dominated failure. In contrast, the GMA maintains nearly radius-independent adhesion up to r = 5 mm and extends this strong-adhesion regime to macroscopic radii of up to 20 mm (Fig. S9, A), consistent with DMT-like detachment, while retaining its performance over more than 50 repeated loading cycles (Fig. S9, B). Observations of the detachment process for 3-mm-radius samples show that PDMS and

Ecoflex detach progressively from the edge through crack propagation (Fig. 3B). In contrast, the GMA promotes central cavitation as interfacial stress builds during pull-off, which becomes unstable upon reaching a critical size and triggers sudden failure.

Finite element analysis (FEA) was performed to investigate the detachment mechanics of a GMA sample with r = 0.5 mm. Cross-sectional (top row) and interfacial (bottom row) views of the normal stress distribution (σ_z) at selected displacements (U_z = 0, 45, 60, 120, and 600 μm) are depicted in Fig. 3C. As U_z increases, the interfacial stress builds uniformly from the center outward and approaches theoretical strength (σ_{th}) across the entire contact area. At U_z = 120 μm, the stress is nearly uniform at σ_{th}, corresponding to the peak adhesion force and consistent with DMT-like behavior. Further loading leads to uniform detachment (e.g., at U_z = 600 μm), with the interfacial stress dropping to zero. The size effect is investigated by comparing the normalized interfacial stress ($\sigma_{\max}/\sigma_{\mathrm{th}}$) at radii of 0.1 mm and 5 mm for GMA, PDMS, and Ecoflex (Fig. 3D, Supplementary Note 5). All adhesives operate in the DMT-regime at r = 0.1 mm, exhibiting nearly uniform stress at failure ($\sigma_{\max}/\sigma_{\mathrm{th}} \sim 1$). As the radius increases, PDMS and Ecoflex progressively develop strong edge-localized stress concentration (Fig. S12). At r = 5 mm, GMA still maintains a uniform stress distribution, with $\sigma_{\max}/\sigma_{\mathrm{th}} = 0.97$ at failure, whereas PDMS and Ecoflex decrease to 0.71 and 0.56, respectively, leading to reduced adhesion. At this radius, finite-thickness effects also raise the center stress in PDMS, giving a mixed detachment mode in which cavitation nucleates at the center, followed by concurrent growth of both central and edge cracks (Fig. S10).

We further examined the shape effects using samples of the same contact areas (~ 78.5 mm^2, equivalent to r = 5 mm) to evaluate their ability to maintain uniform interfacial stress and adhesion strength (Fig. 3E). PDMS and Ecoflex samples exhibit significant decreases in adhesion for complex shapes with sharp corners, with star-shaped samples exhibiting reductions of 31.8% and 41.8%, respectively. In contrast, the GMA maintains nearly consistent adhesion across all shapes, demonstrating excellent shape insensitivity. FEA simulations of normal stress distribution (σ_z) for square and star shaped samples further illustrate this contrast (Fig. 3F, Supplementary Note 6), showing

that the GMA maintains a nearly uniform stress distribution even at sharp corners, whereas PDMS and Ecoflex develop stress concentrations at corners, leading to premature detachment. Compared with commercial adhesives, the GMA uniquely combines high adhesion with shape insensitivity ($\sigma_{\mathrm{star}}/\sigma_{\mathrm{circular}} \sim 1$), demonstrating robust adhesion that is inaccessible to conventional soft adhesives (Fig. 3G).

Surface roughness strongly degrades the adhesion of conventional soft elastomers, as surface asperities induce interfacial stress concentration and reduce effective contact area and adhesion energy. For PDMS, adhesion strength drops sharply as the root mean square (RMS) roughness increases from 0.0492 to 16.4 μm (Fig. S17, Supplementary Note 7), whereas Ecoflex exhibits a more gradual decrease owing to its lower modulus partially mitigating stress concentrations, though its adhesion still degrades at high roughness. GMA, in contrast, sustains strong adhesion across the entire roughness range, with adhesion strength even slightly increasing at higher roughness. This superior performance arises from its modulus gradient, which homogenizes interfacial stress and suppresses asperity-induced stress concentrations, ensuring uniform and stable contact formation even on microscopically irregular surfaces. Substrate material and surface energy strongly influence adhesive performance. In Fig. S18, PDMS and Ecoflex exhibit substantially reduced adhesion on different substrates, especially wood and Teflon. GMA, however, consistently maintains high adhesion (> 639 kPa), even on rough wood and low-surface-energy Teflon, highlighting its exceptional adaptability to challenging surfaces.

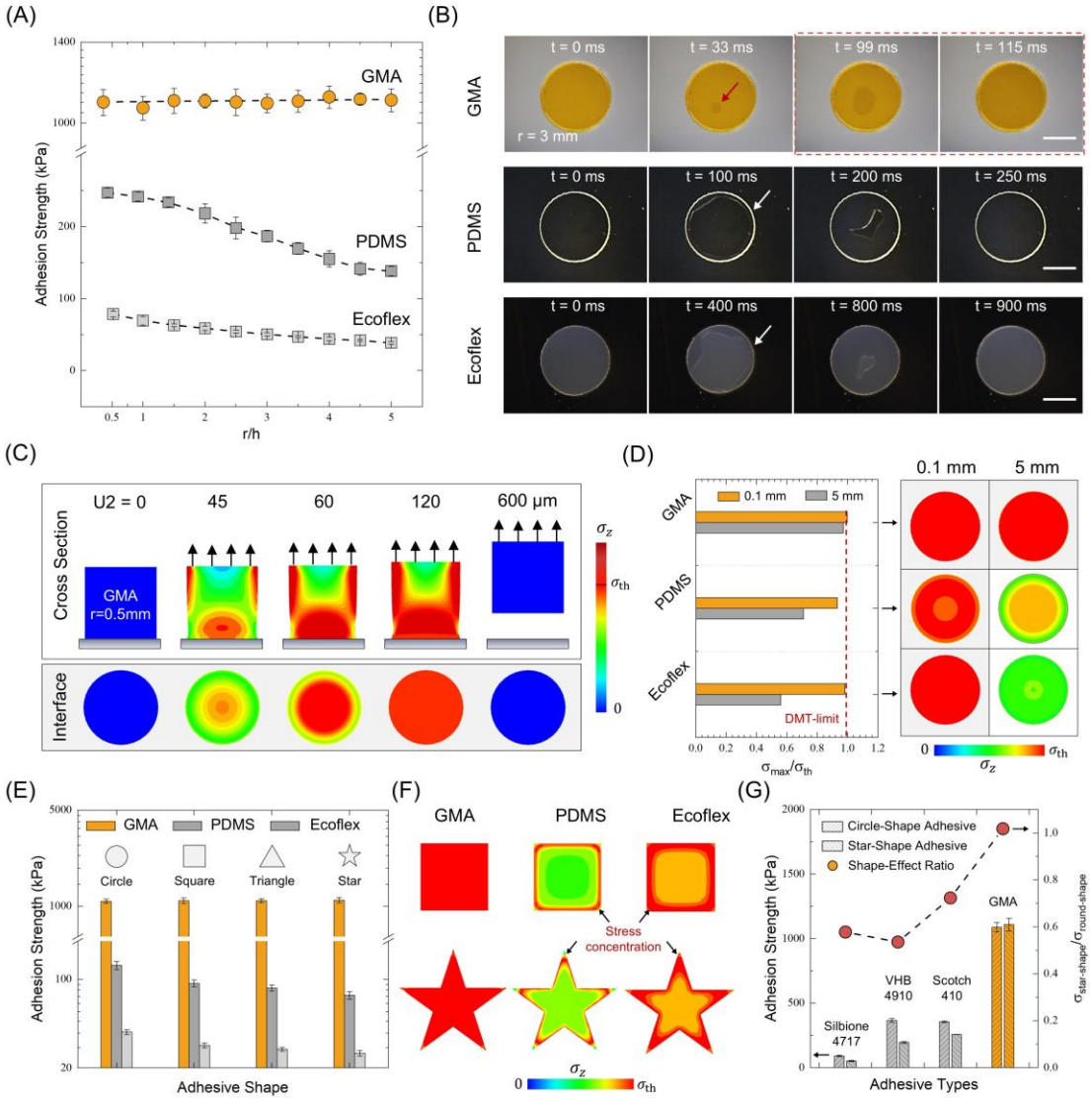


Figure 3. DMT-like adhesion of GMAs across size and shape variations. (A) Experimental measurements of the adhesion strength of GMA, PDMS, Ecoflex on a smooth glass (RMS = 0.0492 μm) as a function of radius-to-thickness ratio (r/h). (B) Optical images capturing the detachment process of GMA, PDMS, Ecoflex with a radius of r = 3 mm. (C) Finite element analysis (FEA) of the normal stress distribution (σ_z) during the detachment process of GMA (r = 0.5 mm). Top: Cross-sectional stress profiles at different vertical displacement. Bottom: Corresponding interfacial stress distributions. (D) FEA results showing the influence of size on the interfacial stress distributions for GMA, PDMS, and Ecoflex at radii of 0.1 mm and 5 mm. Left: Normalized maximum interfacial stress (σ_{max}/σ_{th}) data. Right: Colormaps showing the interfacial stress distributions (σ_z). (E) Adhesion strength of GMA, PDMS, Ecoflex with various shapes (circle, square, triangle, star) under identical contact area. (F) FEA simulation results of σ_z distributions for square and star shapes. (G) Comparison of adhesion switchability and adhesion strength between existing switchable soft adhesives (E < 10 MPa) and GMA.

Thermally switchable adhesion of GMA

Our GMA not only provides strong adhesion but also good switchability for on-demand attachment and detachment. We tested a 5-mm-radius GMA sample at room

temperature (RT) and 80 ℃ (Fig. S19), yielding adhesion forces of 87.86 N and 10.41 N, respectively (Fig. 4A). The force-time curves reveal distinct detachment behaviors. At RT, detachment occurs abruptly at the peak force with a sharp drop, whereas at 80 ℃, adhesion weakens and detachment proceeds gradually as the force decreases over time. This temperature-dependent transition is attributed to the thermally induced phase transition which weakens the modulus gradient at 80 ℃ (above the glass transition temperature, Fig. 2F), and transforms the GMA into a nearly homogenous material, eliminating the advantages of graded modulus design. Consequently, GMA loses its size- and shape-insensitivity, giving rise to switching ratio ($\sigma_{\mathrm{RT}}/\sigma_{80\,℃}$) of 8.44 and 15.38 for circular and star-shaped samples (Fig. 4B). FEA simulations corroborate this mechanism (Supplementary Note 8). By altering the modulus gradient before and after heating, the interfacial von Mises stress distribution shifts from a uniform pattern to one dominated by pronounced edge stress concentration (Fig. 4C). This mechanically driven change in stress distribution directly underlies the thermally switchable adhesion of GMA. The reversibility of this thermal switching is demonstrated by repeated heating-cooling cycles on a low-surface-energy PTFE substrate (Fig. 4D), in which the GMA reproducibly switches between a high-adhesion state at RT and a weak-adhesion state at 80 ℃ over 5 cycles without performance degradation. Across reported switchable soft adhesives (Fig. 4E, Table S1), adhesives with Young's modulus (E) below 10 MPa exhibit an inverse correlation between adhesion strength and switchability, with adhesion strength rarely exceeding 400 kPa. By leveraging a modulus- and shape-modulated transition, GMA represents a significant advance toward high-performance soft adhesives that combine strong adhesion with large switchability.

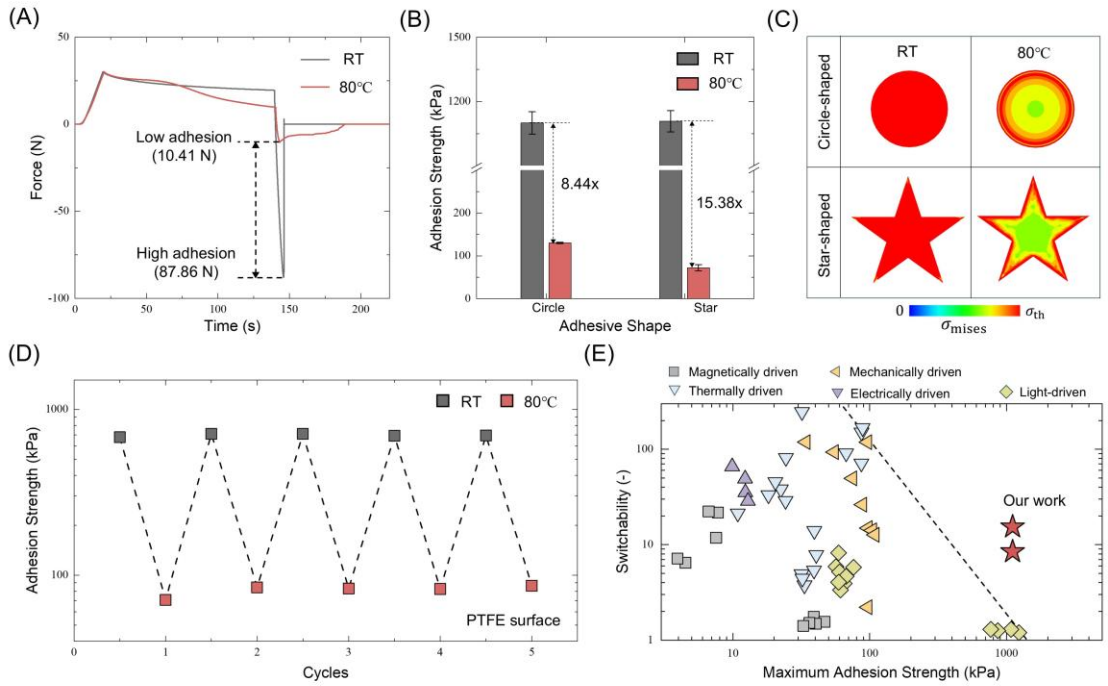


Figure 4. Thermally switchable adhesion of GMA. (A) Force-time curves of a circle-shaped GMA sample (radius = 5 mm) tested at RT and 80 ℃. (B) Adhesion strength of circle- and star-shaped GMA samples at RT and 80 ℃. (C) FEA simulation of interfacial von Mises stress distribution for circle- and star-shaped GMA samples before (RT) and after (80 ℃) thermal erasure of the modulus gradient. (D) Reversible thermal switching of GMA adhesion on a PTFE surface. (E) Comparison of adhesion switchability and adhesion strength between GMA and existing switchable soft adhesives (E < 10MPa).

Demonstrations of GMA performance in comparison

To highlight potential applications of graded modulus design, we benchmarked GMA against widely used commercial 1-mm-thick double-sided tapes (Supplementary Note 9). GMA consistently outperformed all commercial tapes across five key metrics (Fig. 5A, Table S2), including adhesion on low-surface-energy PTFE and rough glass (RMS = 16.4 μm), shape-effect ratio ($\sigma_{\mathrm{star}}/\sigma_{\mathrm{circular}}$), adhesion switchability ($\sigma_{\mathrm{RT}}/\sigma_{80\,℃}$), and adhesion durability. Benefiting from its excellent adhesion performance, GMA formed stable interfaces with a wide range of objects, from curved ball shells to rough bricks and heavy flat steel blocks, maintaining reliable adhesion across diverse weights, geometries, and surface roughness (Fig. 5B).

The adhesion lifetime of GMA was further quantified, showing nearly two orders of magnitude improvement over 3M VHB 4910 tapes under equivalent stress (Fig. 5C). Leveraging its thermally switchable adhesion, GMA was integrated into a

programmable pick-and-place platform (Fig. 5D, Fig. S20). The adhesive rapidly gripped a 500 g steel ball within 10 s, delivered it to a target location and released it upon heating to 80 °C (Supplementary Video 1). The platform also manipulated a 500 g curved steel block (Supplementary Video 2), demonstrating adaptability across different surface curvatures and masses. A handheld device using a star-shaped GMA with enhanced switching ratio was further developed (Fig. 5E), enabling manipulation of objects difficult to grasp, such as 40 mm-radius steel shells (Supplementary Video 3) and flat acrylic sheet (Supplementary Video 4). It also demonstrated reliable repeatability by grasping and releasing a rough wooden cube over five consecutive cycles within 10 s each, without performance degradation (Fig. S21, Supplementary Video 5). Similar results were obtained with cubes of various materials (including iron, Teflon, plastic, glass, and wood, Fig. 5E i-v), highlighting the versatility, repeatability, and broad applicability of the GMA-enabled pick-and-place system (Supplementary Video 6).

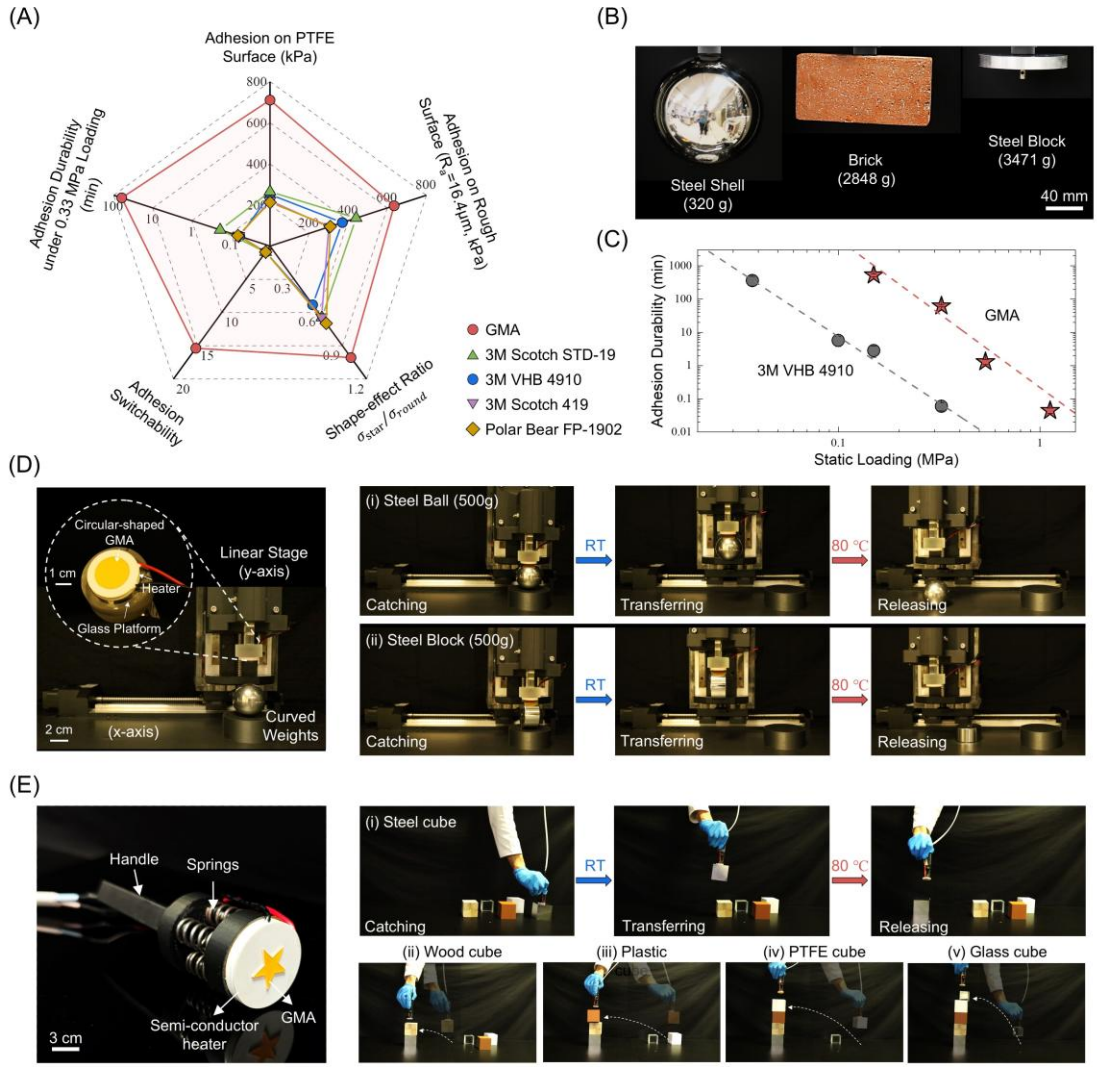


Figure 5. Demonstrations of GMA performance in diverse application scenarios. (A) Benchmarking of GMA adhesion performance against four commercial tapes (3M Scotch STD-19, 3M VHB 4910, 3M Scotch 419, and Polar Bear FP-1902), measured under a preload of 30 N and a short contact time of 2 min. (B) Adhesion of GMA to large and heavy objects with varied surface morphologies, including a steel shell (320 g), brick (2848 g), and steel block (3471 g). (C) Long-term static adhesion comparison between GMA and 3M VHB 4910 tape. (D) Schematic illustration of a two-axis motorized system integrating a heater and GMA as a thermally switchable pick-and-place platform for manipulating a 500 g steel ball (i) and a 500 g curved steel block (ii), enabling multidirectional transport and thermally triggered release at 80 °C. (E) Handheld pick-and-place device incorporating a star-shaped GMA for repeated capture and release of five objects made of different materials: steel (1700 g), Teflon (530 g), plastic (70 g), glass (504 g), and wood (60 g).

Discussion

Our GMA establishes a unified, scalable platform that overcomes long-standing challenges in soft adhesives by simultaneously achieving geometry-independent strong adhesion, robust interfacial conformity, and thermally switchable release.

A continuous modulus gradient, engineered through a one-step photopolymerization

process, suppresses interfacial stress concentration, enabling consistent DMT-like adhesion across contact areas up to 1200 mm^2 and complex geometries. Unlike previous approaches that rely on microstructures or contact splitting, the performance of GMA arises purely from the gradient material design, simplifying fabrication and broadening the materials selection window.

In addition to strong and robust adhesion, the thermally induced phase transition weakens the modulus gradient and enables programmable switching between strong and weak adhesion, allowing rapid, residual-free release and adaptive pick-and-place manipulation across objects with diverse sizes, shapes, curvature, and surface morphologies. This transition allows a detachment mechanism shift from DMT-like to JKR-like, yielding large and tunable switching ratios without compromising integrity or repeatability. Benchmarking against state-of-the-art commercial adhesive tapes highlights the versatility of GMA as it maintains strong adhesion on both rough and low-surface-energy substrates, sustains static loads for a period of more than 2 orders of magnitude longer, and enables fast, reversible detachment through thermally induced weakening of the modulus gradient. These advances position GMA as a new material paradigm for next-generation wearable devices, robotics, and soft-gripping systems.

Methods

Fabrication of the GMA samples: The photocurable acrylic-based resin was prepared by mixing 2-hydroxyethyl acrylate (Aladdin, China), isobornyl acrylate (Aladdin, China), and urethane diacrylate oligomers (UDA, CN9021 NS, Sartomer, USA) at a weight ratio of 20:60:20. A photoinitiator (Irgacure 2022, BASF, 3 wt%) and a photoabsorber (Sudan I, Aladdin, China, 0.02 wt%) were subsequently added. UV curing was performed using a parallel UV light source (405 nm, F224-10.1, Anlun Optics, China), with the source–substrate distance controlled by a custom displacement stage and light intensity monitored with a UV meter (LS125, Linshang, China). The 1 mm-deep resin tank, made of black acrylic to allow top-side illumination only, was filled with resin, covered with a 1.5 mm-thick transparent acrylic sheet, and secured with four clips. The assembly was exposed to UV light at 44.5 mW/cm^2 for 20 s. After

curing, the tank was separated from the cover, leaving the GMA attached to the cover sheet owing to the higher-modulus surface formed adjacent to it. The soft side was rinsed three times with isopropyl alcohol and dried in an oven at 60 °C for 2 h. Finally, GMA samples were cut into designated sizes and geometries using a CO_2 laser cutter (MIRA7, AEON Laser, China) for subsequent testing.

Fabrication of the control group samples: PDMS (Sylgard 184, Dow Corning, USA; 10:1 ratio), Ecoflex 00-30 (Smooth-On, USA; 1:1 ratio), and Dragon Skin 10 (Smooth-On, USA; 1:1 ratio) were cast into a 1 mm-deep resin tank, covered with a 1.5 mm-thick transparent acrylic sheet, clamped at four corners, and cured in an oven at 80 °C for 2 h. For commercial tapes, including VHB 4910, Scotch 410, and Scotch STD-19 (3M, USA) as well as transparent acrylic tape (FP-1902, Polar Bear Co., Ltd., China), the protective liners were removed and both sides re-covered with release paper to enable laser cutting. All samples were subsequently patterned into designated sizes and geometries using a CO_2 laser cutter (MIRA7, AEON Laser Co., Ltd., China) for testing.

Fourier Transform Infrared Spectroscopy Measurements: All FTIR measurements were carried out in attenuated total reflection (ATR) mode using a Nicolet iS50 spectrometer (Thermo Fisher Scientific, Waltham, MA, USA).

Tensile tests: Room-temperature tensile tests were performed on a universal testing machine (Instron 5566, Instron Inc., USA) at a displacement rate of 100 μm/s. High-temperature tests (80 °C) were conducted on a dynamic mechanical analyzer (Q800, TA Instruments, USA) at the same rate. To evaluate the Young's modulus at different positions within the GMA, 0.15 mm-thick films were prepared under varying light intensities and patterned into dog-bone strips (ASTM D1708-18) using a laser cutter. Young's modulus was extracted from the initial linear portion (0.3% strain) of the stress–strain curve obtained from spline fits.

Surface Morphology Characterization: The morphology of smooth and rough glass substrates was measured using a surface profiler (TalyScan 150, Taylor Hobson, Inc.) at a scanning speed of 100 μm/s over a 1 × 1 mm^2 area.

Adhesion Test: Adhesion strength was measured using a universal testing machine (Instron 5566, Instron Inc., USA) equipped with a custom-built tilting stage to ensure

sample alignment and a load cell to record adhesion force. Samples were brought into contact with a glass substrate (RMS = 0.0492 μm) at 10 μm/s until the preload stabilized, then held for 2 min before detachment at a constant speed of 100 μm/s. For thermal switching tests, samples were placed on a heating stage and heated to 80 °C once the preload was reached, after which the adhesion force was recorded under heated conditions. Comparative tests were also performed on PDMS and Ecoflex.

Author contributions

Y. Liu, C. Linghu, and K.J. Hsia conceived the idea. Y. Liu, Y. Yang, W. Liu, S. Hong, B. Teo, Z. Lu, Y. Zhang, and Y. Guo prepared the adhesives and performed the experiments. Y. Liu, Y. Yang, and C. Linghu carried out the FEA simulations. Y. Liu, Y. Yang, Y. Fu, and X. Yang prepared and conducted the programmable pick-and-place demonstrations. Y. Liu, Y. Yang, C. Linghu, E. Arzt and K.J. Hsia analyzed the results. Y. Liu drafted the manuscript with input from Y. Yang, W. Liu, C. Linghu, H. Yu, and X. Wang. Y. Liu, C. Linghu, E. Arzt and K.J. Hsia revised the manuscript. C. Linghu and K.J. Hsia supervised the study and provided funding acquisition.

Competing interests

The authors declare that they have no competing interests.

Acknowledgements

K.J.H. acknowledges the support by the Ministry of Education (MOE) of Singapore under Academic Research Fund tier 2 (MOE-T2EP50122-0001) and a research start-up grant (002271-00001) from the Nanyang Technological University. C. L. acknowledge the support by a grant from City University of Hong Kong (Project No. 9382018) and Program of Key Laboratory of Low Dimensional Materials and Application Technology (Xiangtan University) of Ministry of Education No. 2025ZD03. S.H. acknowledge the support by URECA project from the Nanyang Technological University. E.A. acknowledges support by the Tan Chin Tuan Foundation during a research stay at NTU.

References

[1] H. Yuk, J. Wu, X. Zhao, Hydrogel interfaces for merging humans and machines, *Nature Reviews Materials* **2022**, 7, 935-952.

[2] C. Linghu, S. Zhang, C. Wang, et al., Universal SMP gripper with massive and selective capabilities for multiscaled, arbitrarily shaped objects, *Science Advances* **2020**, 6, eaay5120.

[3] Y. Liu, X. Li, H. Yang, et al., Skin-Interfaced Superhydrophobic Insensible Sweat Sensors for Evaluating Body Thermoregulation and Skin Barrier Functions, *ACS Nano* **2023**, 17, 5588-5599.

[4] J. Zhao, X. Li, Y. Tan, et al., Smart Adhesives via Magnetic Actuation, *Adv Mater* **2022**, 34, e2107748.

[5] D. Hwang, C. Lee, X. Yang, et al., Metamaterial adhesives for programmable adhesion through reverse crack propagation, *Nature Materials* **2023**, 22, 1030-1038.

[6] C. Linghu, Z. Du, Y. Sun, et al., On shear adhesion of adhesive fibrils, *Extreme Mechanics Letters* **2023**, 64, 102092.

[7] A. Luo, K. T. Turner, Achieving enhanced adhesion through optimal stress distributions, *Journal of the Mechanics and Physics of Solids* **2021**, 156, 104610.

[8] A. Luo, K. T. Turner, Mechanics of crack path selection in microtransfer printing: Challenges and opportunities for process control, *Journal of the Mechanics and Physics of Solids* **2020**, 143, 104066.

[9] H. Gao, H. Yao, Shape insensitive optimal adhesion of nanoscale fibrillar structures, *Proceedings of the National Academy of Sciences* **2004**, 101, 7851-7856.

[10] L. F. Boesel, C. Greiner, E. Arzt, et al., Gecko-inspired surfaces: a path to strong and reversible dry adhesives, *Adv Mater* **2010**, 22, 2125-2137.

[11] D. R. King, M. D. Bartlett, C. A. Gilman, et al., Creating gecko-like adhesives for "real world" surfaces, *Adv Mater* **2014**, 26, 4345-4351.

[12] B. Peng, X.-Q. Feng, Q. Li, Decohesion of a rigid flat punch from an elastic layer of finite thickness, *Journal of the Mechanics and Physics of Solids* **2020**, 139,

103937.

[13] C. Linghu, X. Yang, Y. Liu, et al., Mechanics of shape-locking-governed R2G adhesion with shape memory polymers, *Journal of the Mechanics and Physics of Solids* **2023**, 170, 105091.

[14] B. V. Derjaguin, V. M. Muller, Y. P. Toporov, Effect of contact deformations on the adhesion of particles, *Journal of Colloid and Interface Science* **1975**, 53, 314-326.

[15] R. G. Balijepalli, M. R. Begley, N. A. Fleck, et al., Numerical simulation of the edge stress singularity and the adhesion strength for compliant mushroom fibrils adhered to rigid substrates, *International Journal of Solids and Structures* **2016**, 85-86, 160-171.

[16] K. L. Johnson, K. Kendall, A. D. Roberts, Surface energy and the contact of elastic solids, *Proceedings of the Royal Society of London. A. Mathematical and Physical Sciences* **1997**, 324, 301-313.

[17] F. Jin, X. Guo, H. Gao, Adhesive contact on power-law graded elastic solids: The JKR–DMT transition using a double-Hertz model, *Journal of the Mechanics and Physics of Solids* **2013**, 61, 2473-2492.

[18] M. Kamperman, E. Kroner, A. del Campo, et al., Functional Adhesive Surfaces with “Gecko” Effect: The Concept of Contact Splitting, *Advanced Engineering Materials* **2010**, 12, 335-348.

[19] D. Sameoto, Beyond biomimicry - next generation applications of bioinspired adhesives from microfluidics to composites, *Beilstein J Nanotechnol* **2024**, 15, 965-976.

[20] E. Arzt, H. Quan, R. M. McMeeking, et al., Functional surface microstructures inspired by nature – From adhesion and wetting principles to sustainable new devices, *Progress in Materials Science* **2021**, 120, 100823.

[21] M. Bacca, J. A. Booth, K. L. Turner, et al., Load sharing in bioinspired fibrillar adhesives with backing layer interactions and interfacial misalignment, *Journal of the Mechanics and Physics of Solids* **2016**, 96, 428-444.

[22] S. Song, D. M. Drotlef, C. Majidi, et al., Controllable load sharing for soft

adhesive interfaces on three-dimensional surfaces, *Proc Natl Acad Sci U S A* **2017**, 114, E4344-E4353.

[23] Z. Wang, Slanted Functional Gradient Micropillars for Optimal Bioinspired Dry Adhesion, *ACS Nano* **2018**, 12, 1273-1284.

[24] C. Linghu, Y. Liu, X. Yang, et al., Fibrillar adhesives with unprecedented adhesion strength, switchability and scalability, *National Science Review* **2024**, 11, nwae106, .

[25] M. Chen, Y. Wu, B. Chen, et al., Fast, strong, and reversible adhesives with dynamic covalent bonds for potential use in wound dressing, *Proc Natl Acad Sci U S A* **2022**, 119, e2203074119.

[26] R. Li, D. Li, J. Sun, et al., Pull-off dynamics of mushroom-shaped adhesive structures, *Journal of the Mechanics and Physics of Solids* **2024**, 183, 105519.

[27] R. Hensel, K. Moh, E. Arzt, Engineering Micropatterned Dry Adhesives: From Contact Theory to Handling Applications, *Advanced Functional Materials* **2018**, 28, 1800865.

[28] S. Kim, A. Carlson, H. Cheng, et al., Enhanced adhesion with pedestal-shaped elastomeric stamps for transfer printing, *Applied Physics Letters* **2012**, 100, 171909.

[29] S. N. Gorb, M. Varenberg, Mushroom-shaped geometry of contact elements in biological adhesive systems, *Journal of Adhesion Science and Technology* **2007**, 21, 1175-1183.

[30] S. S. Pande, K. T. Turner, Geometric optimization of pillars for enhanced adhesion, *Extreme Mechanics Letters* **2023**, 59, 101969.

[31] R. G. Balijepalli, S. C. L. Fischer, R. Hensel, et al., Numerical study of adhesion enhancement by composite fibrils with soft tip layers, *Journal of the Mechanics and Physics of Solids* **2017**, 99, 357-378.

[32] S. C. Fischer, E. Arzt, R. Hensel, Composite Pillars with a Tunable Interface for Adhesion to Rough Substrates, *ACS Appl Mater Interfaces* **2017**, 9, 1036-1044.

[33] C. J. Stabile, K. T. Turner, High Strength and Dynamically Tunable Adhesion Enabled by Composite Micropillar Arrays Fabricated via Solvent-Assisted

Molding, *Advanced Materials Technologies* **2024**, 10, 2401588.

[34] H. K. Minsky, K. T. Turner, Achieving enhanced and tunable adhesion via composite posts, *Applied Physics Letters* **2015**, 106, 201604

[35] H. K. Minsky, K. T. Turner, Composite Microposts with High Dry Adhesion Strength, *ACS Appl Mater Interfaces* **2017**, 9, 18322-18327.

[36] H. Tian, D. Wang, Y. Zhang, et al., Core-shell dry adhesives for rough surfaces via electrically responsive self-growing strategy, *Nature Communications* **2022**, 13, 7659.

[37] D. Wang, T. Liu, H. Tian, et al., Stiffness-gradient adhesive structure with mushroom-shaped morphology via electrically activated one-step growth, *Proc Natl Acad Sci U S A* **2025**, 122, e2423039122.

[38] B. Zhu, D. Tan, K. Xiao, et al., Micropillar with Radial Gradient Modulus Enables Robust Adhesion and Friction, *Small* **2024**, 20, e2310887.

[39] H. Cho, G. Wu, J. Christopher Jolly, et al., Intrinsically reversible superglues via shape adaptation inspired by snail epiphragm, *Proc Natl Acad Sci U S A* **2019**, 116, 13774-13779.

[40] C. Linghu, Y. Liu, Y. Y. Tan, et al., Overcoming the adhesion paradox and switchability conflict on rough surfaces with shape-memory polymers, *PNAS* **2023**, 120, e2221049120.

[41] C. Linghu, Y. Liu, X. Yang, et al., Versatile adhesive skin enhances robotic interactions with the environment, *Science Advances* **2025**, 11, eadt4765.

[42] A. J. Kinloch, in *Adhesion and adhesives: science and technology*, Springer Science & Business Media, 2012.

[43] Z. Liu, M. A. Meyers, Z. Zhang, et al., Functional gradients and heterogeneities in biological materials: Design principles, functions, and bioinspired applications, *Progress in Materials Science* **2017**, 88, 467-498.

[44] S. Suresh, Graded Materials for Resistance to Contact Deformation and Damage, *Science* **2001**, 292, 2447-2451.

[45] H. Yao, H. Gao, Gibson-Soil-Like Materials Achieve Flaw-Tolerant Adhesion, *Journal of Computational and Theoretical Nanoscience* **2010**, 7, 1299-1305.

[46] H. Yao, H. Gao, Mechanical principles of robust and releasable adhesion of gecko, *Journal of Adhesion Science and Technology* **2007**, 21, 1185-1212.

[47] P. Zhang, H. Ruan, Q. Li, et al., Resolving hyperelasticity-adhesiveness conflict in polymer networks by in situ constructing mechanical heterogeneities, *Nat Commun* **2025**, 16, 6094.

[48] A. B. M. T. Haque, D. H. Ho, D. Hwang, et al., Electrically Conductive Liquid Metal Composite Adhesives for Reversible Bonding of Soft Electronics, *Advanced Functional Materials* **2023**, 34, 2304101.

[49] X. Zhang, X. Li, Scaling Effect of Dry Adhesion for Microfibrils and Transition Size to Flaw Insensitivity, *Journal of Applied Mechanics* **2023**, 90.

[50] Z. Zhao, J. Wu, X. Mu, et al., Origami by frontal photopolymerization, *Science Advances* **2017**, 3, e1602326.

[51] A. Vitale, M. G. Hennessy, O. K. Matar, et al., Interfacial Profile and Propagation of Frontal Photopolymerization Waves, *Macromolecules* **2014**, 48, 198-205.

Supplementary Files

This is a list of supplementary files associated with this preprint. Click to download.

- SupplementaryVideo1.mp4
- SupplementaryVideo3.mp4
- SupplementaryVideo4.mp4
- SISoftAdhesiveStrengthenedbyGradedDesignclean.pdf
- SupplementaryVideo6.mp4
- SupplementaryVideo5.mp4
- SupplementaryVideo2.mp4